Neural Networks 21 (2008) 654–666

Contents lists available at ScienceDirect

Neural Networks

journal homepage: www.elsevier.com/locate/neunet

2008 Special Issue

Powered ankle-foot prosthesis to assist level-ground and stair-descent gaits

Samuel Au [a], Max Berniker [a], Hugh Herr [a,b,*]

[a] MIT Media Laboratory, 20 Ames Street, Cambridge, MA 02139, USA

[b] The Harvard-MIT Division of Health Sciences and Technology, 20 Ames Street, Cambridge, MA 02139, USA

ARTICLE INFO

Article history:
Received 23 July 2007
Received in revised form
7 March 2008
Accepted 7 March 2008

Keywords:
Powered prosthesis
Amputee gait
Myoelectric control
Impedance control

ABSTRACT

The human ankle varies impedance and delivers net positive work during the stance period of walking. In contrast, commercially available ankle-foot prostheses are passive during stance, causing many clinical problems for transtibial amputees, including non-symmetric gait patterns, higher gait metabolism, and poorer shock absorption. In this investigation, we develop and evaluate a myoelectric-driven, finite state controller for a powered ankle-foot prosthesis that modulates both impedance and power output during stance. The system employs both sensory inputs measured local to the external prosthesis, and myoelectric inputs measured from residual limb muscles. Using local prosthetic sensing, we first develop two finite state controllers to produce biomimetic movement patterns for level-ground and stair-descent gaits. We then employ myoelectric signals as control commands to manage the transition between these finite state controllers. To transition from level-ground to stairs, the amputee flexes the gastrocnemius muscle, triggering the prosthetic ankle to plantar flex at terminal swing, and initiating the stair-descent state machine algorithm. To transition back to level-ground walking, the amputee flexes the tibialis anterior muscle, triggering the ankle to remain dorsiflexed at terminal swing, and initiating the level-ground state machine algorithm. As a preliminary evaluation of clinical efficacy, we test the device on a transtibial amputee with both the proposed controller and a conventional passive-elastic control. We find that the amputee can robustly transition between the finite state controllers through direct muscle activation, allowing rapid transitioning from level-ground to stair walking patterns. Additionally, we find that the proposed finite state controllers result in a more biomimetic ankle response, producing net propulsive work during level-ground walking and greater shock absorption during stair descent. The results of this study highlight the potential of prosthetic leg controllers that exploit neural signals to trigger terrain-appropriate, local prosthetic leg behaviors.

© 2008 Elsevier Ltd. All rights reserved.

1. Introduction

Today's commercially available transtibial prostheses are completely passive during stance, and consequently their stance-phase mechanical properties remain fixed with walking speed and terrain. Such prostheses typically comprise elastic bumper springs or carbon composite leaf springs that store and release energy during the stance period, e.g. the College Park or Flex-Foot (Ron, 2002). In distinction, the human ankle is known to vary impedance within each level-ground walking cycle, across walking speed, and during stair descent and ascent (Gates, 2004; Hansen, Childress, Miff, Gard, & Mesplay, 2004; Palmer, 2002; Winter, 1983). Furthermore, studies have indicated that one of the main functions of the human ankle is to provide adequate energy for forward progression of the body (Gates, 2004; Hansen et al., 2004; Hof, Geelen, & Van den Berg, 1983; Palmer, 2002; Winter, 1983). Not surprisingly, transtibial amputees experience many problems when using passive-elastic prostheses, including non-symmetric gait patterns, higher metabolic ambulatory rates, and poorer shock absorption (Bateni & Olney, 2002; Colborne, Naumann, Longmuir, & Berbrayer, 1992; Molen, 1973; Skinner et al., 1985; Winter & Sienko, 1988). To better mimic the human ankle-foot complex and to improve clinical efficacy, a prosthetic ankle-foot mechanism must actively control joint impedance and non-conservative motive power during stance, while at the same time not exceeding the weight of the missing limb.

Several engineering challenges hinder the development of a powered ankle-foot prosthesis (Au, Dilworth, & Herr, 2006; Koganezawa & Kato, 1987; Winter & Sienko, 1988). With current actuator technology, it is challenging to build an ankle-foot prosthesis that matches the size and weight of the human ankle-foot complex, but still provides sufficient stance-period work and instantaneous power output to propel an amputee forward. Ankle-foot mechanisms for humanoid robots are often too heavy or not sufficiently powerful to meet the biomimetic specifications

* Corresponding author at: MIT Media Laboratory, 20 Ames Street, Room 424, Cambridge, MA 02139, USA. Tel.: +1 617 314 3661; fax: +1 617 253 8542.
E-mail address: hherr@media.mit.edu (H. Herr).

0893-6080/$ – see front matter © 2008 Elsevier Ltd. All rights reserved.
doi:10.1016/j.neunet.2008.03.006

required for a powered prosthesis (Hirai et al., 1998; Kaneko et al., 2004). Furthermore, a powered prosthesis must be position and impedance controllable. Often, robotic ankle controllers follow pre-planned kinematic trajectories during walking (Hirai et al., 1998; Kaneko et al., 2004), whereas the human ankle is believed to operate in impedance control mode during stance and position control mode during swing (Gates, 2004; Hansen et al., 2004; Palmer, 2002). Finally, it is challenging to measure and respond to the amputee's movement intent. For some time, researchers have attempted to use myoelectric signals measured from residual limb musculature as control commands for an external prosthesis or exoskeleton (Abul-haj & Hogan, 1990; Akazawa, Okuno, & Yoshida, 1996; Farry et al., 1996; Fukuda et al., 2003; Graupe et al., 1978; Huang & Chen, 1999; Rosen et al., 2001). However, due to the nonlinear and non-stationary characteristics of the myoelectric signal (Abul-haj & Hogan, 1990; Akazawa et al., 1996; Farry et al., 1996; Fukuda et al., 2003; Graupe et al., 1978; Huang & Chen, 1999; Rosen et al., 2001), researchers have only been able to provide position *or* impedance control, whereas a prosthetic ankle-foot system requires a continuous joint control where both position *and* impedance are actively modulated.

Some recent research has focused on the development of quasi-passive ankle-foot prostheses. Researchers have built prostheses that use active damping or spring-clutch mechanisms to allow automatic ankle angle adjustment for distinct ground surfaces (Hansen et al., 2007; Li et al., 2006; Ossur, 2002–2008; US Patent 6443993, 2002), or to allow for an improved metabolic walking economy (Collins & Kuo, 2003). Since these devices do not include an actuator to actively plantar flex the ankle at terminal stance, no net work is performed throughout each walking step, as is the case with the human ankle (Gates, 2004; Hansen et al., 2004; Hof et al., 1983; Palmer, 2002; Winter, 1983). In 1998, Klute and colleagues (Klute, Czerniecki, & Hannaford, 1998) were the first to build a powered ankle-foot prosthesis capable of performing net positive work. Their device employed a pneumatic actuation strategy with offboard power. Recently, Versluys and colleagues (Versluys et al., 2007) also designed a powered prosthesis with pneumatic actuation and offboard power. Other recent work has focused on the design of energetically-autonomous powered systems (Au, 2007; Au, Bonato, & Herr, 2005; Au & Herr, 2006; Au, Weber, & Herr, 2007a, in review; Au, Weber, Martinez-Villapando, & Herr, 2007b; Herr, Paluska, Dilworth, & Au, 2005; Herr, Weber, & Au, 2007; Hitt, Bellman, Holgate, Sugar, & Hollander, 2007). In this investigation, we further develop the powered ankle-foot design described in Au (2007), Au et al. (2005), Au and Herr (2006), Au et al. (2007a), Au et al. (in review), Au et al. (2007b), Herr et al. (2005) and Herr et al. (2007).

A long-term objective in the field of prosthetic leg design is to advance artificial joints that mimic the dynamics of the missing limb, not only for level-ground gait patterns, but also for irregular terrain ambulation. In this investigation, we seek a prosthetic intervention that captures biomimetic gait patterns for two terrain surfaces, namely level-ground and stairs. To this end, we build a powered prosthesis that comprises a unidirectional spring, configured in parallel with a force-controllable actuator with series elasticity. The prosthesis employs both sensory inputs measured local to the external prosthesis, and myoelectric inputs measured from residual limb muscles. Using local prosthetic sensing of joint state and ground reaction force, we develop two finite state controllers to produce biomimetic gait patterns for level-ground and stair-descent walking. To transition between these gaits, myoelectric signals measured from the tibialis anterior and gastrocnemius muscles are used as control commands. We conduct a pilot clinical evaluation to test whether the finite state controllers result in a more biomimetic ankle response. Specifically, we measure prosthetic ankle state, torque, and power during level-ground and stair descent using both the proposed controllers and a conventional passive-elastic control. Finally, we test whether the amputee participant can robustly and accurately transition between the state controllers through direct muscle activation.

2. Methods

In this section, we first review human ankle biomechanics for both level-ground and stair-descent gaits. Motivated by these biomechanics, we then describe the design of the finite state controllers for both gaits. Additionally, we present a terrain detection approach where myoelectric signals measured from an amputee's residual limb muscles are used to infer his/her intent on the choice of local state machine controllers. In this discussion, we include methods used for acquiring the myoelectric signals, and the algorithm employed to infer motor commands based on these signals. Finally, we describe the experimental protocol used in a preliminary clinical evaluation of the prosthetic intervention.

2.1. Human ankle biomechanics

2.1.1. Level-ground walking

A level-ground walking cycle is typically defined as beginning with the heel strike of one foot and ending at the next heel strike of the same foot (Inman, Ralston, & Todd, 1981). The main subdivisions of the gait cycle are the stance phase (60% gait cycle) and the swing phase (40% gait cycle) (See Fig. 1). The swing phase (SW) represents the portion of the gait cycle when the foot is off the ground. The stance phase begins at heel strike when the heel touches the floor and ends at toe-off when the same foot rises from the ground surface. From (Gates, 2004; Palmer, 2002), the stance phase of walking can be divided into three subphases: Controlled Plantar Flexion (CP), Controlled Dorsiflexion (CD), and Powered Plantar Flexion (PP). These phases of gait are described in Fig. 1. Detailed descriptions for each subphase are provided below.

Controlled Plantar Flexion (CP)

CP begins at heel strike and ends at foot flat. Simply speaking, CP describes the process by which the heel and forefoot initially make contact with the ground surface. Within a CP phase, ankle torque is proportional to ankle position, but ankle stiffness does change between walking steps. Thus, CP mechanics have been modeled as a linear spring with variable stiffness from step to step (Gates, 2004; Palmer, 2002).

Controlled Dorsiflexion (CD)

CD begins at foot flat and continues until the ankle reaches a state of maximum dorsiflexion. The main function of the human ankle during CD is to store elastic energy to help propel the body during the phase of powered plantar flexion. Ankle torque versus position during the CD period is often described as a nonlinear spring where stiffness increases with increasing ankle position (Gates, 2004; Hansen et al., 2004; Palmer, 2002; Winter, 1983).

Powered Plantar Flexion (PP)

PP begins after CD and ends at the instant of toe-off. As the positive work generated during PP is more than the negative work absorbed during the CP and CD phases for moderate to fast walking speeds (Gates, 2004; Hansen et al., 2004; Hof et al., 1983; Palmer, 2002; Winter, 1983), additional energy is supplied along with the spring energy stored during the CD phase to achieve the high plantar flexion power during late stance (Fig. 1B). Thus, during PP the ankle has been modeled as a torque source in parallel to a CD spring (Gates, 2004; Palmer, 2002).

Swing Phase (SW)

SW begins at toe-off and ends at heel-strike. It represents the portion of the gait cycle when the foot is off the ground. Here the ankle position is modulated until the landing ankle position is achieved at terminal SW. Thus, the ankle can be modeled as a position source during this phase.

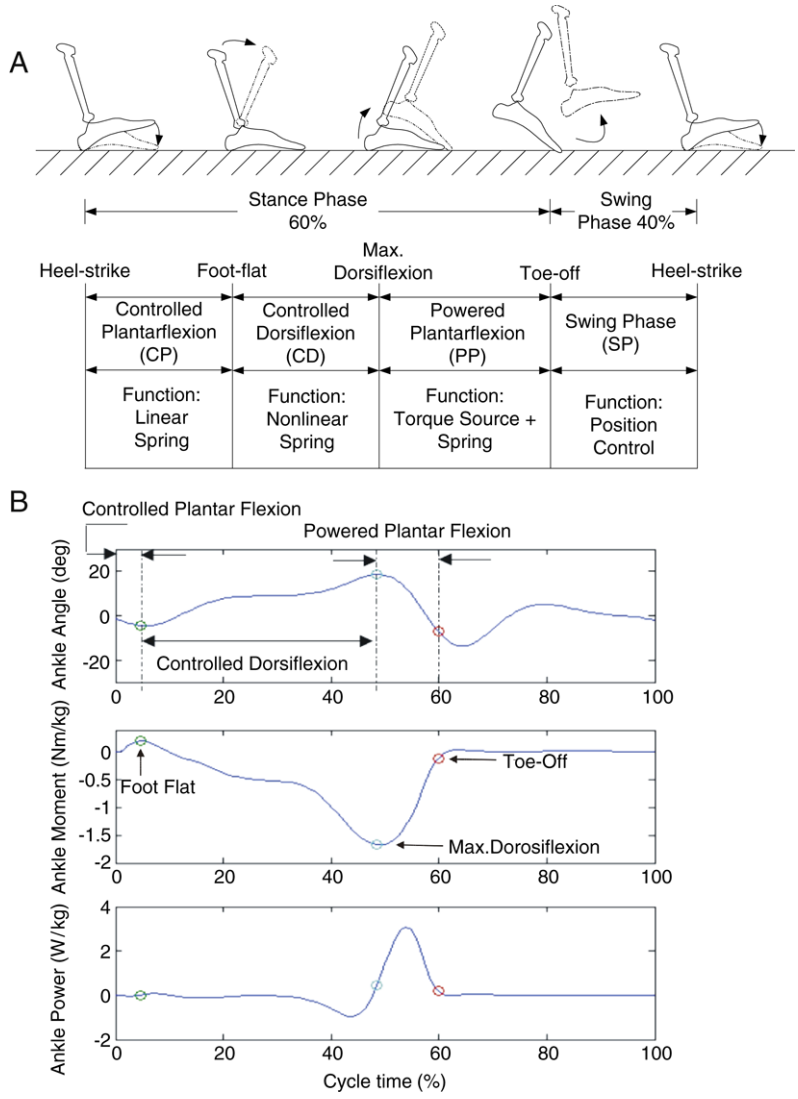

Fig. 1. Human ankle biomechanics for level-ground walking. In (A), a description of normal human ankle biomechanics are provided as a function of walking gait phase. In (B), a representative plot of ankle angle, moment, and power for level-ground walking are plotted versus percent gait cycle for a normal healthy individual walking at a self-selected speed (reproduced with permission from Gates (2004)). Ankle moment and power are normalized by body mass. Zero percent cycle corresponds to heel strike and 100% to heel strike of the same leg. Circles denote important gait events.

2.1.2. Stair-descent walking

Human ankle biomechanics for stair descent are significantly different from that of level-ground walking. A stair-descent gait cycle is typically defined as beginning with the toe-strike of one foot and ending at the next toe-strike of the same foot (Gates, 2004; McFadyen & Winter, 1988; Riener, Rabuffetti, & Frigo, 2002). The stance phase of stair descent is divided into three subphases: Controlled Dorsiflexion 1 (CD1), Controlled Dorsiflexion 2 (CD2), and Powered Plantar Flexion (PP). These phases of gait are described in Fig. 2. Detailed descriptions for each subphase are provided below.

Controlled Dorsiflexion 1 (CD1)

CD1 begins at toe-strike and ends at foot flat. In this phase, the forefoot strikes the next stair tread initially with the ankle in a plantar flexed position (Fig. 2A). During this phase, a significant amount of potential energy is absorbed as the body is lowered onto the step. The power absorbed during this phase is always negative and is not followed by a period of positive power (Fig. 2B). Thus, CD1 mechanics have been modeled as a variable damper (Gates, 2004; McFadyen & Winter, 1988; Riener et al., 2002).

Controlled Dorsiflexion 2 (CD2)

CD2 starts at foot flat and continues until the ankle reaches a maximum dorsiflexion posture. Here, the ankle has been modeled as a linear spring in parallel with a variable damper so as to effectively control the amount of energy absorbed (Gates, 2004).

Powered Plantar Flexion (PP)

PP begins at maximum dorsiflexion and ends at toe-off. In this phase, the ankle releases the elastic energy stored during CD2 to propel the body upwards and forwards. Thus, like CD2 the ankle has been modeled as a linear spring in parallel with a variable damper (Gates, 2004).

Swing Phase (SW)

SW begins at toe-off and ends at toe-strike. For stair descent, the ankle is plantar flexed by -0.35 rad ($-20°$) when the foot first makes contact with the stair tread at toe-strike. Here again as in level-ground walking, the ankle can be modeled as a position source.

2.1.3. Summary of human ankle biomechanics

In this investigation, we develop a powered ankle-foot prosthesis to address the following three functions of the human ankle:

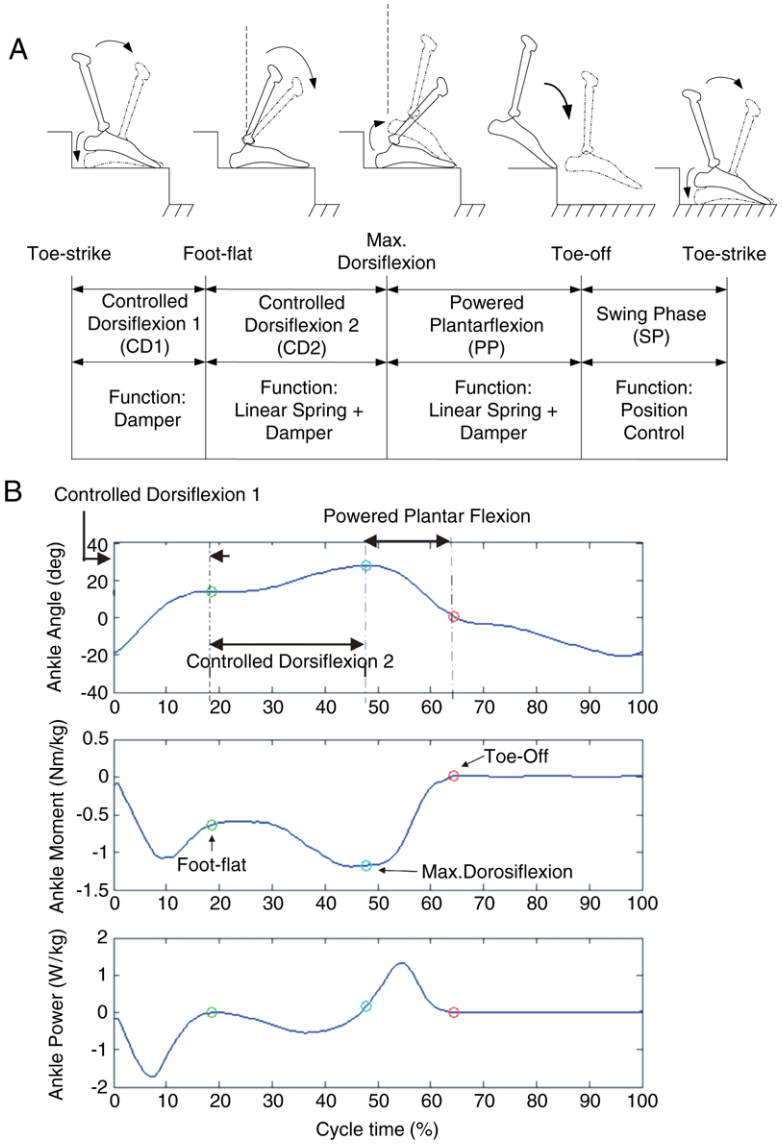

Fig. 2. Human ankle biomechanics for stair descent. In (A), a description of normal human ankle biomechanics is provided as a function of stair-descent gait phase. In (B), a representative plot of ankle angle, moment, and power for stair descent are plotted versus percent gait cycle for a normal healthy individual walking at a self-selected speed (reproduced with permission from Gates (2004)). Data normalizations are equivalent to those used in Fig. 1.

(i) the human ankle modulates joint impedance (joint stiffness and damping) during the stance phase of walking; (ii) the ankle provides net positive work during the stance period of level-ground walking; and (iii) the ankle behaves as a position source to control the foot orientation during the swing phase. The above human ankle properties define the basic functional requirements of the powered ankle-foot prosthesis, and motivate the target prosthesis behavior of the control system.

2.2. MIT powered ankle-foot prosthesis

Motivated by human ankle biomechanics, we developed a powered ankle-foot prosthesis to study amputee–machine interaction (see Fig. 3) (Au, 2007; Au et al., 2007a, in review, 2007b; Herr et al., 2007). The prosthesis was capable of varying impedance during the stance period of walking, in a similar manner to a normal human ankle. In addition, it provided a sufficiently large instantaneous power output and torque to propel an amputee during PP, while still matching the size and weight of an intact limb. Providing sufficient power output from a relatively small and lightweight device has been argued as the dominant design hurdle in the development of a powered ankle-foot prosthesis (Koganezawa & Kato, 1987; Winter, 1983; Winter & Sienko, 1988).

For the powered prosthesis presented here, the basic architecture of the electromechanical mechanism was a physical spring, configured in parallel to a high-power, force-controllable actuator with series elasticity. There were five main mechanical components in the system: a high-power output DC motor, a transmission, a series spring, a unidirectional parallel spring, and a carbon composite prosthetic foot (see Fig. 3C). We combined the first three components, including the DC motor, transmission, and the series spring, to form a rotary Series-Elastic Actuator (SEA). The SEA (Pratt & Williamson, 1995; Robinson, 2000) consisted of a motor in series with a spring (or spring structure) via a mechanical transmission. The SEA provided force control through the modulation of series spring compression. Using a linear potentiometer, we obtained the force applied to the load by measuring the deflection of the series spring. The SEA was used to modulate the joint stiffness/damping as well as to provide the motive power output for

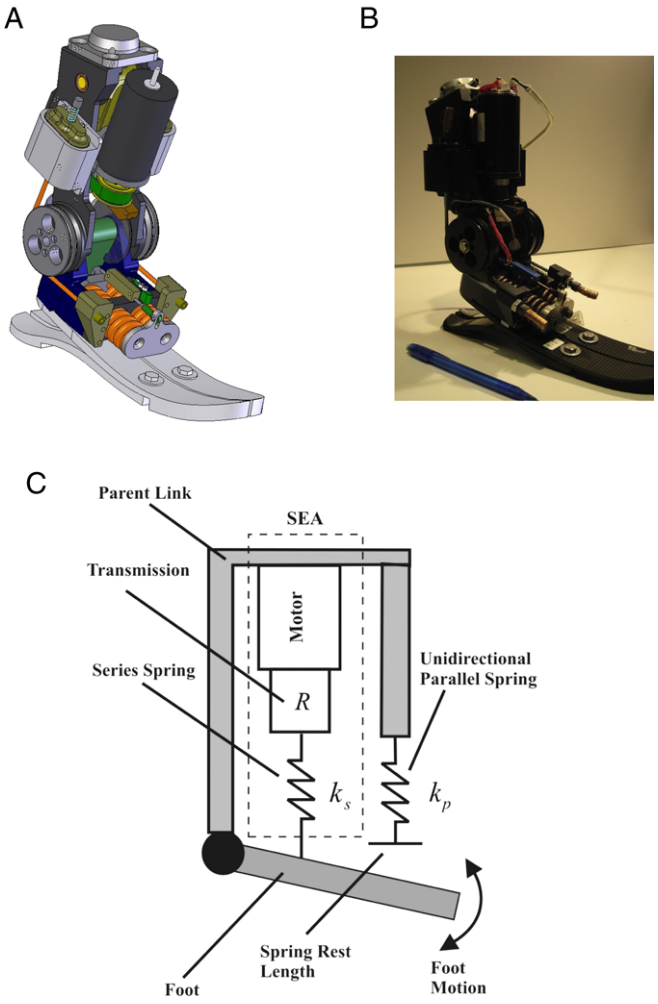

Fig. 3. Powered ankle-foot prosthesis. In (A), a CAD model is shown, and in (B), the physical prototype. In (C), a schematic of the prosthetic architecture is shown. The prosthesis comprises a series-elastic actuator in parallel with a unidirectional spring.

active push-off (Au, 2007; Au & Herr, 2006; Au et al., 2007a, in review, 2007b; Herr et al., 2007). Owing to the demanding power and torque requirements of an ankle-foot prosthesis (Au et al., 2007a; Koganezawa & Kato, 1987; Winter, 1983; Winter & Sienko, 1988), we incorporated a physical spring, configured in parallel to the SEA, so that the load borne by the SEA could be greatly reduced. Owing to this parallel elasticity, the SEA had a sufficient large force bandwidth that provided the active push-off during PP. To avoid hindering the foot motion during plantar flexion, the parallel spring was implemented as a unidirectional spring that provided an offset stiffness value only when the ankle angle was larger than zero radians, or when the ankle was dorsiflexed. Since the main focus of this paper is on prosthetic ankle control design and evaluation, the details of the mechanical design and component selections are not addressed here. Additional information can be found in Au (2007), Au et al. (2007a), Au et al. (in review), Au et al. (2007b) and Herr et al. (2007).

2.3. Myoelectric-driven finite state control

2.3.1. Overall architecture

Finite state controllers have often been used in leg orthotic and prosthetic devices, such as knee prostheses (Grimes, 1976; Herr & Wilkenfeld, 2003; Koganezawa & Kato, 1987; Zlatnik, Steiner, & Schweitzer, 2002), because leg gait patterns are typically repetitive between strides and within a stride, and can be characterized into distinct subphases. In this investigation, such regular gait patterns motivated the usage of a finite state architecture to control a powered ankle-foot prosthesis.

Based on the biomechanical descriptions in Section 2.1, we now specify five basic goals for the control design of a powered ankle-foot prosthesis.

- A finite state controller should contain sufficient numbers of states to replicate the functional behaviors of a gait pattern.
- Three types of low-level servo controllers are required to mimic basic ankle behaviors: (i) a torque controller; (ii) an impedance controller; and (iii) a position controller.
- Local mechanical sensing on the external prosthesis is desirable for both gait detection and transitions among states. A finite state controller is sought that uses external prosthetic sensory information to manage the state transitions and to determine which low-level servo controller to employ in order to provide proper prosthetic function within any given state.
- Due to fundamental biomechanical differences between level-ground and stair-descent gaits, two separate finite state controllers are required.
- A high-level control input is sought to manage transitions between the finite-state controllers for level-ground and stair-descent gaits.

In this investigation, a control system with two separate finite state controllers was implemented to provide human ankle behaviors for both level-ground and stair-descent gaits. The overall architecture of the control system is shown in Fig. 4. First, the control system contained the suggested, three low-level servo controllers to mimic basic human ankle functions. Second, only local variables were adopted for state detection and transition, including ankle angle, torque and foot contact pressure. Third, one finite state controller was designed for level-ground walking, while a second was designed for stair descent. Fourth, we used myoelectric signals measured from residual limb muscles of an amputee as control commands to manage the switching between the finite state controllers (Fig. 4). A Myoelectric Processing Unit was designed to detect an amputee's intent on the controller transition. This intent detection was based on muscular activities (myoelectric signals) measured on the residual limb surface. To transition from level-ground walking to stair descent, the amputee flexed his/her gastrocnemius muscle during the swing phase of walking. Once a Myoelectric Processing Unit detected the corresponding muscle activity pattern, it then triggered the prosthetic ankle to plantar flex at terminal swing and initiated the stair-descent state machine algorithm. To transition back to level-ground walking, the amputee flexed his/her tibialis anterior during the swing phase, changing the foot landing condition and initiating the level-ground state machine algorithm.

In the next sections, we first describe the design of the finite state controllers for level-ground and stair-descent gaits. We then discuss in Section 2.4 how myoelectric signals were employed to determine the switching between the proposed finite state controllers. Finally, we discuss the details of the control system implementation and hardware development in Section 2.5. Since the main focus of this paper is on the design and implementation of the finite state controllers, and the switching between them, a detailed description of the low-level servo controllers is not provided. Further information on this topic can be found in Au (2007) and Au et al. (in review).

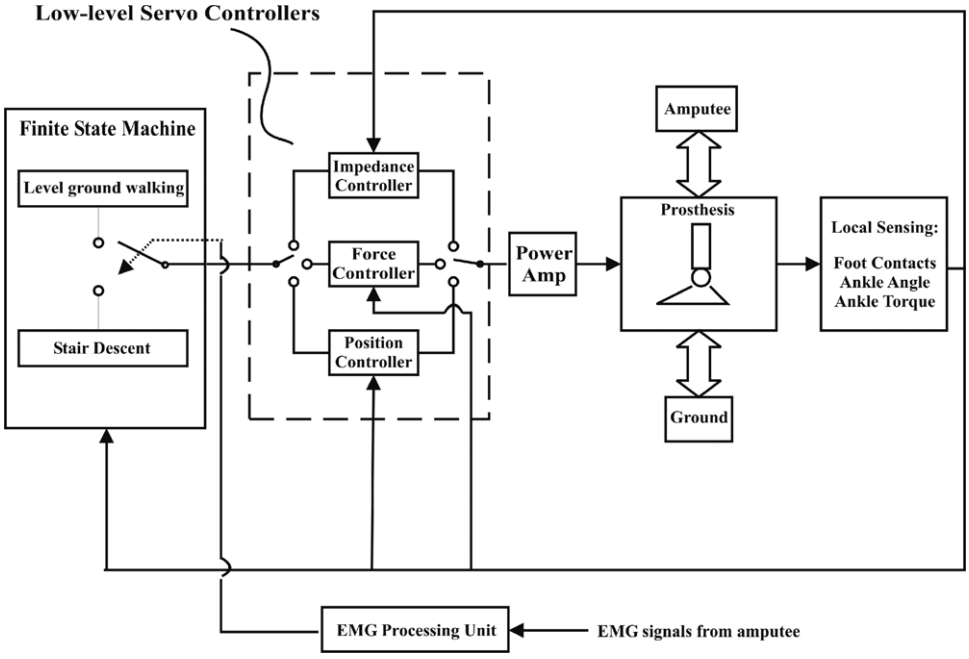

Fig. 4. Overall control system architecture.

2.3.2. Finite state control for level-ground walking

Stance-phase control

A finite state controller for level-ground walking was implemented based on the biomechanical descriptions in Section 2.1.1 (see Fig. 5A). Three states were designed for stance-phase control, which were named CP, CD and PP. For ease of implementation, we made a couple of modifications in state definitions and desired state behaviors, as compared to those described in Section 2.2.1. Descriptions for each state of the stance-phase control are as follows.

- CP begins at heel-strike and ends at mid-stance when the ankle angle is equal to zero. During CP, the prosthesis outputs a joint stiffness K_{CP}[1] to prevent forefoot slapping and to provide shock absorption during heel-strike.
- CD begins at mid-stance and ends at either toe-off, or when the measured total ankle torque T_{ankle} is larger than a predefined torque threshold τ_{pp}($T_{ankle} > \tau_{pp}$). During CD, the prosthesis outputs a total joint stiffness K_{CD} to allow a smooth rotation of the body. The total joint stiffness is $K_{CD} = K_P + K_{CD1}$, where K_P, K_{CD1} are the rotary stiffness components contributed by the parallel spring and the SEA, respectively.
- Once again, PP begins only when the measured ankle torque T_{ankle} is larger than a predefined torque threshold τ_{pp} ($T_{ankle} > \tau_{pp}$). Otherwise, it remains in state CD until the foot comes off the ground. During PP, the prosthesis outputs a constant offset torque $\Delta\tau$, as an active push-off, superimposed on joint stiffness K_{CD}.

K_{CP}, K_{CD}, τ_{pp}, $\Delta\tau$ were the main parameters affecting ankle performance during the stance phase. In particular, the offset torque $\Delta\tau$ was related to the amount of net work done at the ankle joint. These parameter values were chosen based on biomechanical information and the amputee's preferences during experiments (see Section 2.6.1 *Experimental Protocol*).

[1] The conversion of joint stiffness between translational and rotary domains is $K_{=}r^2k$, where k and r are the translational joint stiffness and the moment arm, respectively. For example, $K_{CP} = r^2 k_{CP}$.

Swing phase control

Another three states (SW1, SW2, and SW3) were designed for the swing phase control. Descriptions for each state are as follows.

- SW1 begins at toe-off and ends in a given time period t_H. During SW1, the prosthesis servos the foot to a predefined foot position θ_{toeoff} for foot clearance.
- SW2 begins immediately after SW1 and finishes in a time period t_2. During SW2, the amputee is allowed to voluntarily control the equilibrium position of the foot for a time period, t_2, as a means of selecting an appropriate finite state controller. The amputee's motor intent is determined from available myoelectric signals. In this application, the motor intent is only inferred to a binary output foot position, θ_{EMG}: (i) $\theta_{EMG} = 0$ implies the amputee's intent for level-ground walking, and (ii) $\theta_{EMG} = -0.35$ rad ($-20°$) implies the amputee's intent for stair descent. The output foot position θ_{EMG} is then sent to the position controller as the desired equilibrium position, θ_d, and the controller servos the foot to that desired position within the time period t_2. Once the time period t_2 is over, the controller determines whether the system should stay in the level-ground walking mode, or stair-descent mode, depending on the current equilibrium position θ_d. When $\theta_d \geq 0$, the state control enters state SW3 of the level-ground walking mode. Otherwise, the system switches to the stair-descent mode and enters state CD1.
- SW3 begins immediately after SW2 and ends at the next heel-strike. During SW3, the state controller resets the system to impedance mode and outputs a joint stiffness K_{CP}.

Time periods t_H and t_2, and predefined foot position θ_{toeoff}, were all tuned experimentally. It was important to have state SW3 in the swing phase control to ensure that the control system operated in impedance mode before heel-strike. Owing to the rapid impact of heel-strike, there was insufficient time for the control system to switch from position control to impedance control at the instant of foot strike.

Sensing for state transitions

During state transition and identification, the system mainly relied on four variables:

- Heel contact (H). $H = 1$ indicates that the heel is on the ground, and vice versa.

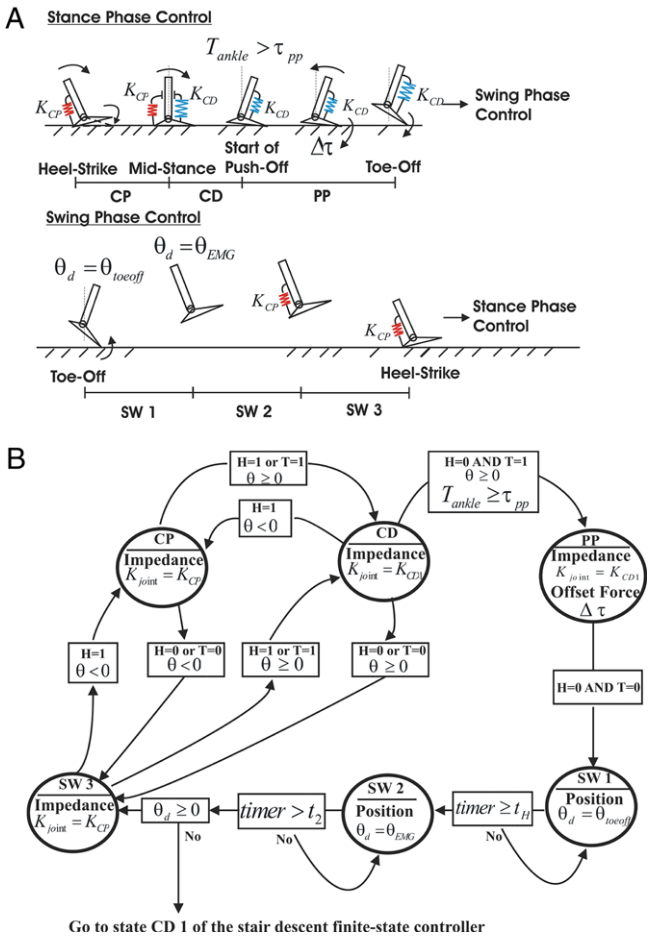

Fig. 5. Finite state controller for level-ground walking. In (A), the desired prosthesis behavior for level-ground walking is depicted for both stance and swing phases. In (B), the finite state machine is shown with state control actions and transitional conditions noted.

- Toe contact (T). $T = 1$ indicates that the toe is on the ground, and vice versa.
- Ankle angle (θ)
- Total ankle torque (T_{ankle}).

All of the above triggering information was obtained using sensors located on the external prosthesis, including foot switches to measure heel/toe contact, an ankle joint encoder to measure the ankle angle, and a linear spring potentiometer to measure joint torque. The hardware implementation for the local prosthetic sensing is discussed in Section 2.5, and a state machine diagram with all triggering conditions is shown in Fig. 5B.

2.3.3. Finite state control for stair descent

Stance-phase control

Another finite state machine was implemented to provide normal stair-descent walking patterns (see Fig. 6A). Only two states (CD1, CD2) were designed for stance-phase control. We did not implement state PP in the stair-descent controller because, according to Section 2.1.2, human ankle behavior during CD2 is basically the same as that during PP. The modified state definitions and desired state behaviors for the stance-phase control are as follows.

- CD1 begins just before toe-strike and ends at foot flat. During CD1, the prosthesis outputs a joint damping K_{D01} to reduce impact loads generated during toe-strike.

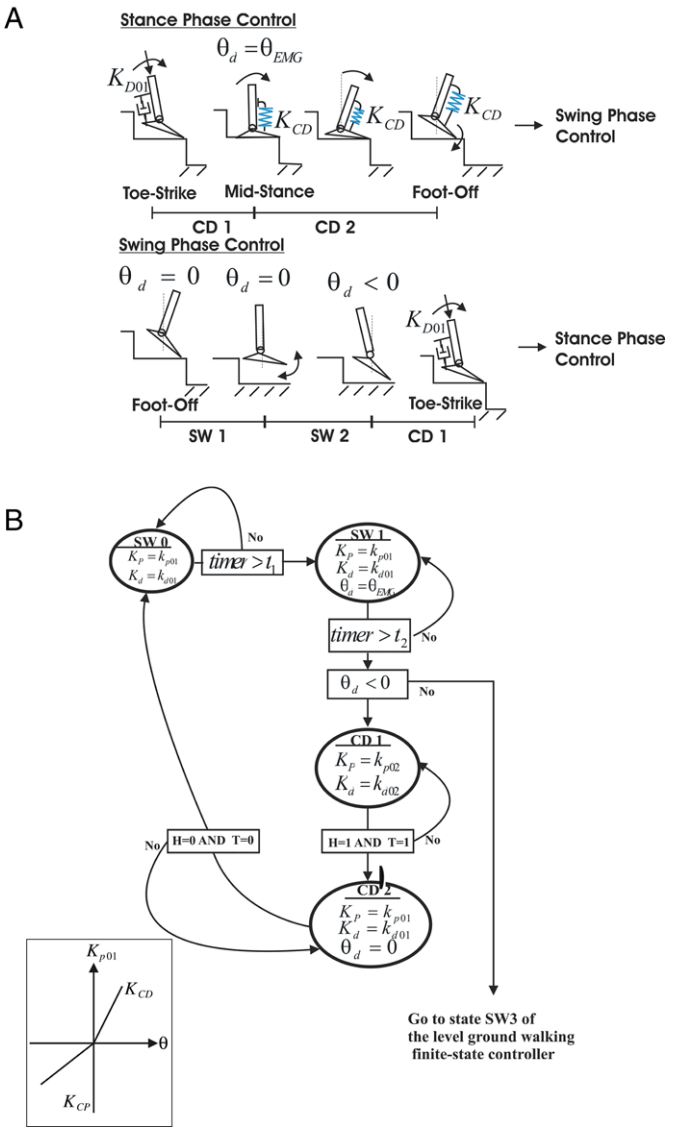

Fig. 6. Finite state control for stair descent. In (A), the desired prosthesis behavior for stair descent is depicted for both stance and swing phases, and in (B), the finite state machine is shown.

- CD2 begins at foot flat and ends at toe-off. During CD2, the prosthesis outputs a joint stiffness K_{CD} (including parallel spring stiffness) when the ankle angle is greater than zero radians. Otherwise, it outputs another joint stiffness, K_{CP}. The prosthesis also resets the equilibrium position of the impedance controller back to zero radians ($\theta_d = 0$).

We did not incorporate the damping component in state CD2 as described in Section 2.1.2 because in general, the damping component in state CD2 is relatively insignificant compared to the stiffness component (Gates, 2004; McFadyen & Winter, 1988). In addition, it is noted that the intrinsic damping in the mechanical transmission contributed adequate damping for stability.

Swing phase control

Two states (SW1, SW2) were designed for the stair-descent swing phase control. Descriptions for each state are as follows.

- SW1 begins at toe-off and ends in a given time period, t_1. During SW1, the prosthesis servos the foot to the default equilibrium position $\theta_d = 0$. This state serves as a buffer for foot clearance before the use of the amputee's motor commands to control foot orientation.

- SW2 begins immediately after SW1 and finishes in a time period t_2. During SW2, the amputee is allowed to voluntarily control the equilibrium position of the foot for a time period, t_2, to select an appropriate finite state controller. As mentioned in Section 2.3.2, if $\theta_{\text{EMG}} = -0.35$ rad or $-20°$ (i.e. $\theta_d \geqslant 0$), the system remains in the stair-descent mode and enters state CD1. Otherwise it switches back to the level-ground walking mode and enters state SW3 of the level-ground walking swing-phase control.

Time periods t_1 and t_2 were both selected experimentally. The corresponding state machine diagram with all triggering conditions is shown in Fig. 6B.

2.4. Myoelectric processing unit

A myoelectric processing unit was designed to detect the amputee's intent on the choice of finite state controllers, based on residual limb muscular activities. Unit inputs were raw myoelectric signals recorded from the gastrocnemius and tibialis anterior muscles of the residual limb. The output was the binary foot position θ_{EMG} which was either 0 or -0.35 rad ($-20°$). Referring to Section 2.3, if $\theta_{\text{EMG}} = 0$ it implied that the amputee intended to employ the level-ground walking mode. Otherwise, the stair-descent finite state controller was used for the next gait cycle. The output foot position θ_{EMG} was then set equal to the equilibrium position θ_d of the position controller to trigger the controller transition. The myoelectric processing unit was comprised of two components: Myoelectric Pre-processing and Neural Network Motor-Intent Estimator. The details of each component are discussed in the next section.

2.4.1. Myoelectric pre-processing

We measured myoelectric signals from those residual limb muscles that had previously actuated the biological ankle before amputation. Using surface electrodes (disposable 22 × 33 mm Ag/AgCl myoelectric medical sensors Grass F-E10ND), we recorded from the gastrocnemius muscle for prosthetic ankle plantar flexion control, and from the tibialis anterior for prosthetic ankle dorsiflexion control. To preprocess the myoelectric signals measured from each electrode, we developed an onboard analog amplification/filtering circuit interface, powered by a dedicated split supply derived from a pair of 9 V batteries. The front-end of the myoelectric amplifier consisted of an Ohmic subject safety isolation (100 K), a differential (3.3 kHz) and common mode filtering (16 kHz), and amplification gain of 25. Later stages applied a gain of 504, a pair of 1st order highpass filters (16 Hz), a 2nd order lowpass (300 Hz), and a final output lowpass filter of 800 Hz. Total system gain, or the dimensionless ratio between the input and output of the myoelectric amplifier, was equal to 12,600. The amputee's reference potential was established by connecting "ground" electrodes through a safety resistance (100K) to the myoelectric amplifier's local "ground". Finally, the outputs of the myoelectric amplifiers were digitized by the PC104 data acquisition system at 2000 Hz.

A 100 ms sliding window was then used to compute a running standard deviation of the myoelectric signal. Many models (Graupe et al., 1978; Hogan, 1976) of myoelectric signal processing assume that the signal is a white noise process whose standard deviation is proportional to the strength of the motor command. Though our control approach did not rely on these specific assumptions, in practice, computing the standard deviation of a myoelectric signal has served as a robust indicator of a muscle's excitation level (Doerschuk, Gustafson, & Willsky, 1983; Farry et al., 1996).

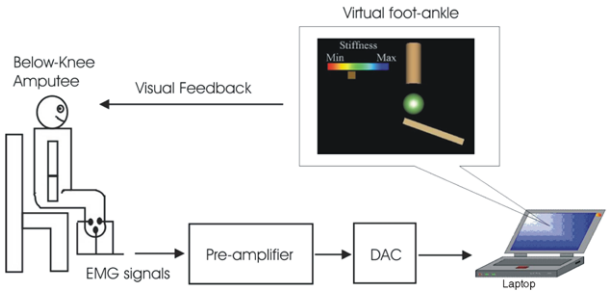

Fig. 7. Schematic of training setup.

2.4.2. Neural network motor-intent estimator

As for our study, we were concerned with making transitions between different motor states. Rather than deducing what could be a continuously varying character of the ankle (McFadyen & Winter, 1988), we inferred the subject's discrete motor intent via the variances of the measured myoelectric signals. In this study, the motor intent was parsimoniously defined by three discrete ankle states: plantar flexed, relaxed, and dorsiflexed.

In order to learn a relationship between myoelectric measurements of the residual muscles and the ankle states, a feed-forward neural network with a single hidden layer was used. The network had a single output for the ankle state, three units in the hidden layer, and one input unit for each myoelectric-derived standard deviation estimate (in most cases, three). Each unit had a nonlinear sigmoidal activation function, ensuring the ability to learn a potentially nonlinear mapping between inputs and ankle state.

To obtain training data for the network, we required both myoelectric signals from residual limb muscles as well as the intended ankle state. A training protocol was developed to capture these input–output pairs of data. Before the experiment, three pairs of surface electrodes were affixed on the participant's residual limb. A first electrode was located over the tibialis anterior, and the second and third electrodes were positioned over the gastrocnemius muscle, on the medial and lateral gastrocnemius heads. After the study participant had surface electrodes suitably located on their limb, they performed a brief training procedure. The participant was shown an iconic representation of an ankle on a computer monitor and asked to mimic a series of displayed orientations (see Fig. 7). Once this procedure was complete, the recorded myoelectric measurements, as well as the presented ankle orientations, were used to train the network. The network was trained using a standard back propagation and gradient descent algorithm.

The motor intent obtained by the NN model y_1 is a continuous number in the range $(-1, 1)$, where -1 is plantar flexion and 1 is dorsiflexion (see Fig. 8). As we were only concerned with making discrete transitions among different motor states, we numerically integrated y_1 and then limited it from -1 to 1. This allowed the participant to toggle between different motor states as they would with a common remote control, i.e. flexing their limb muscles for a brief period of time would signify a transition to a new motor state. The new motor state would persist until the subject flexed the appropriate muscles to switch to another state. We then quantized the new motor state to obtain a discrete motor output command, y_2, whose value can be either -1, 0, or 1.

In our investigation, we were only concerned with motor intent for level-ground walking ($y_2 = 0$, relaxed) and stair descent, ($y_2 = -1$, plantar flexed) in order to use the motor intent to determine the desired output foot position, θ_{EMG}. As can be seen in Fig. 8, if $y_2 < 0$, the Neural Network Motor-Intent Estimator would set $\theta_{\text{EMG}} = -0.35$ rad, otherwise, $\theta_{\text{EMG}} = 0$. The desired output foot position θ_{EMG} was sent to the position controller to adjust the equilibrium position, θ_d, during state SW1 (stair-descent mode)

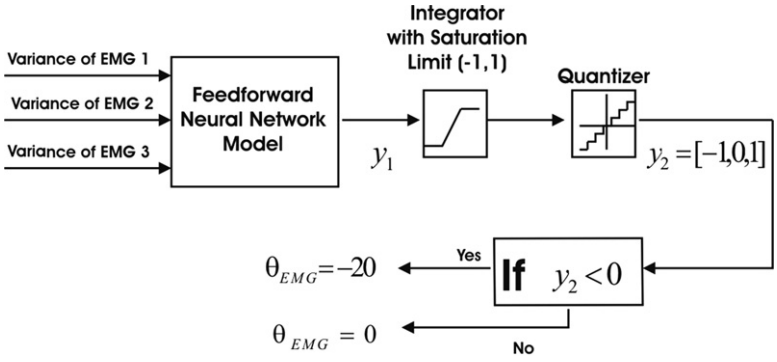

Fig. 8. Neural Network Motor-Intent Estimator. The inputs and output of the system are the variances of myoelectric signals recorded from residual limb muscles and the desired output foot orientation, θ_{EMG}, respectively.

or SW2 (level-ground walking mode). We set $\theta_{EMG} = -0.35$ for stair descent because the human ankle normally plantar flexes to about -0.35 rad ($-20°$) to prepare for toe-strike (Gates, 2004) (See Fig. 2B).

2.5. Hardware implementation

This section describes the electronic hardware used for implementing the proposed controllers on the powered ankle-foot prosthesis, including sensors and the computing platform. The platform provided a test bed for evaluating a broad range of ankle control systems experimentally.

2.5.1. Sensors

Three local state variables, including heel/toe contact, ankle angle, and joint torque, were measured to implement the proposed finite state controllers. We installed a 5 kΩ linear potentiometer across the flexion and extension series springs to measure their displacement. We also mounted a 500-line quadrature encoder (US digital, Inc.) in between the parent link mounting plate and child link mounting plate to measure the joint angle of the prosthetic ankle. Six capacitive force transducers were placed on the bottom of the foot; two sensors beneath the heel and four beneath the forefoot region.

2.5.2. Computing system

Fig. 9A shows the schematics of the computer system. The system contained an onboard computer PC104 with a data acquisition card, power supply, and motor amplifier. The system was powered by a 48 V, 4000 mAh Li-Polymer battery pack. The PC104 used in the study was a MSMP3XEG PC/104 from Advanced Digital Logic, Inc. It was fitted with a PENTIUM III 700 MHz processor. Custom signal conditioning boards amplified sensor (linear pot) readings and provided a differential input to the data acquisition board, in order to minimize common mode noise from pick-up in the system. A PC104 format multifunctional I/O board, Model 526 (from Sensory, Inc) was connected to the PC104 to provide I/O to interface with sensors and motor controller. The system ran the Matlab Kernel for xPC target application. The target PC104 communicated with a host computer via Ethernet. The host computer sent control commands and obtained sensory data from the target PC104. A custom breakout board interfaced the sensors to the D/A board on the PC104 as well as provided power to the signal conditioning boards. The DC motor of the prosthesis was powered by a motor amplifier (Accelnet Panel ACP-090-36, $V = 48$ V, $Ipk = 36$ A) from Copley Controls Corp.

Finally, a mobile computing platform was developed that allowed un-tethered walking outside the laboratory. As shown in Fig. 9B, the mobile platform was mounted on an external frame backpack. Most of the electronic components were mounted on the platform, including the PC104, power supply, I/O Cards, and motor amplifier. Using cabling, the prosthesis was connected to the I/O board and motor amplifier on the platform.

2.6. Clinical study

The objective of the clinical study was to evaluate the robustness and performance of the proposed myoelectric-driven, finite state controller as well as to obtain subjective feedback from an amputee participant. For an initial pilot investigation, we tested the device on a healthy male, bilateral transtibial amputee (age: 40, body mass: 78 kg, height: 180 cm) that wore the powered prosthesis on his right leg and a conventional passive below-knee prosthesis (Flex-Foot Ceterus® from Ossur, Inc.) on his left leg.

We measured the mechanics of the proposed prosthesis while the participant walked at self-selected speeds for two gait patterns: level-ground and stair descent. For each gait pattern, two experimental conditions were examined. In a first experimental condition – the active prosthetic condition (Active) – the powered prosthesis was controlled based on the proposed finite state controllers in Section 2.3. In a second experimental condition – the virtual spring condition (Virtual Spring) – the powered prosthesis was programmed to emulate a passive spring, such as the Flex-Foot. The second experimental condition served as a control to compare the performance between the proposed powered prosthesis and a conventional passive-elastic prosthesis. Initial walking experiments were conducted in the Biomechatronics Group within the MIT Media Lab. The experiments were approved by MIT's Committee on the Use of Humans as Experimental Subjects (COUHES). The participant volunteered for the study and was permitted to withdraw from the study at any time and for any reason. Before taking part in the study, the participant read and signed a statement acknowledging informed consent.

2.6.1. Experimental protocol

The study was divided into two sessions: Myoelectric Training Session and Basic Gait Study. In the Myoelectric Training Session, the input-output training data for the myoelectric training platform was measured and used to train a neural network model to predict the participant's intent. As mentioned in Section 2.4.2, the amputee participant was asked to learn how to control the state transition using his residual muscles. During the experiment, the amputee participant was asked to control the residual muscles to mimic the pre-programmed ankle positions from the graphical display (see Fig. 7). Both myoelectric signals and the corresponding pre-programmed ankle positions were captured during the experiment. The measured data were then used to train a neural network model to infer the participant's motor intent.

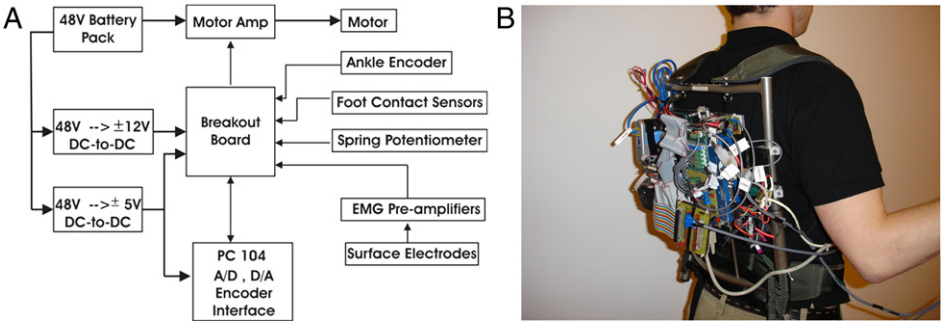

Fig. 9. Seft-contained Computing System. The schematics of the computer system, and a mobile computing platform are shown. The system was designed to provide the capability of testing the prosthesis outside the laboratory.

In the Basic Gait Study, the prosthesis' mechanical behaviors for level-ground walking and stair descent were captured. Before any testing, the participant was fitted with the powered prosthesis by a professional prosthetist. This session was divided into two parts: the first part focused on level-ground walking while the second focused on stair descent. For the level-ground walking experiment, the participant was asked to walk along a 10 m long walkway at his self-selected speed. The prosthesis was first programmed with a virtual spring response with stiffness values (K_{CP}, K_{CD}) from normalized biological data.[2] The prosthetist then further refined the alignment using standard prosthetic alignment procedures. After this alignment phase, each participant was given the option of making adjustments to the desired stiffness values (K_{CP}, K_{CD}) by communicating to a separate operator. The prosthesis was then programmed to output the active torque source response superimposed on the stiffness response during PP as described in Section 2.3.2. The parameter values for the torque source response, including the predefined torque threshold (τ_{pp}) and the offset torque ($\Delta\tau$), were initially set based on normalized biological values. Each participant was then given the option of making adjustments to the torque source parameters (τ_{pp}, $\Delta\tau$) until they achieved the most favorable prosthetic ankle response.

Once control parameters were selected, seven walking trials were recorded for both the Active and Virtual Spring control conditions. For the stair-descent experiment, the participant was asked to descend a flight of stairs with a standard run and rise of 25.5 cm and 18 cm, respectively. Here again, seven walking trials were recorded for both the Active and Virtual Spring control conditions. The participant wore the mobile computing platform throughout all experimental trials, and joint torque and angle sensory data from the prosthesis were recorded.

3. Results

In this section, we first present the results obtained from the clinical gait evaluation of the powered prosthesis for both level-ground and stair-descent gaits. We then show that the proposed neural network motor-intent estimator allowed the amputee to select preferred prosthetic state controllers voluntarily.

3.1. Level-ground Walking

The level-ground finite state machine performed robustly throughout the experimental session. The amputee participant and the prosthetist were satisfied with the performance of the prosthesis. In general, it took less than 20 min for the participant to adapt and feel comfortable with the powered prosthesis.

[2] In Gates (2004), ankle torque was normalized by body mass, and plotted versus ankle position. Thus, to get actual ankle stiffness values, we first multiplied the normalized biological data by the study participant's body mass before taking the slope (stiffness) of the ankle torque-position data.

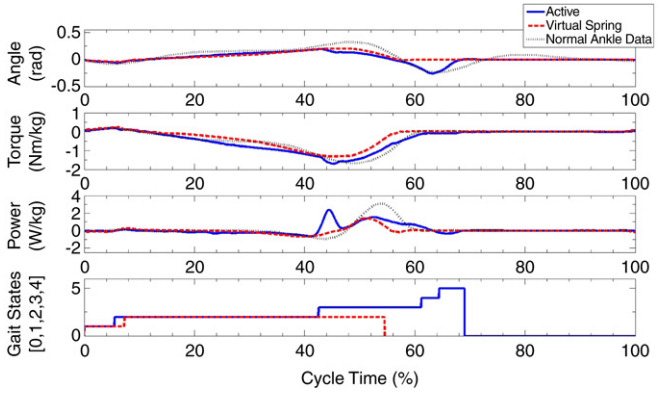

Fig. 10. Prosthetic ankle performance for level-ground walking. The solid blue, dotted red, and dotted grey lines represent the measured gait data for the active prosthetic condition (Active), the virtual spring condition (Virtual Spring), and the human ankle, respectively. The gait states for level-ground walking are defined as follows: CP = 1, CD = 2, PP = 3, SW1 = 4, SW2 = 5, and SW3 = 0. Zero percent cycle corresponds to heel strike and 100% to heel strike of the same leg. Ankle torque and power are normalized by total body mass. (For interpretation of the references to colour in this figure legend, the reader is referred to the web version of this article.)

Fig. 10 shows data for one level-ground walking cycle while using the two experimental conditions: active prosthetic condition (Active) and virtual spring condition (Virtual Spring). The gait states for level-ground walking are defined as follows: CP = 1, CD = 2, PP = 3, SW1 = 4, SW2 = 5, and SW3 = 0. Under the Virtual Spring condition, the system went through the state sequence 1-2-0 (CP-CD-SW3) for each level-ground walking cycle. While under the Active prosthetic condition, the system went through a longer state sequence, or 1-2-3-4-5-0 (CP-CD-PP-SW1-SW2-SW3).

As is shown in Fig. 10, the participant had a longer and more biomimetic stance period associated with the Active condition than with the Virtual Spring condition. Toe-off occurred at 60% gait cycle for the Active control condition, but occurred earlier at 54% gait cycle for the Virtual Spring condition. As shown in Fig. 1, toe-off occurs at 60% gait cycle in normal human walking. It is also noted that the prosthetic ankle angle and torque trajectories under the Active condition were similar to the human trajectories shown in Fig. 1. Specifically, the Active and Virtual Spring conditions resulted in a maximum plantar flexion angle at toe-off equal to -0.170 ± 0.002 and 0.040 ± 0.005 rad, respectively, and a peak torque at terminal stance equal to -1.72 ± 0.01 N m/kg and -1.19 ± 0.06 N m/kg, respectively.

Under the Active condition, the prosthesis demonstrated the capacity to deliver net positive work and high mechanical power during stance. However, as shown in Fig. 10, two power splits or hubs are present at terminal stance for the prosthesis that do not appear in human walking. The average net work performed by the prosthesis for both the Active and Virtual Spring conditions were $+12.5 \pm 0.1$ J and $+0.18 \pm 0.06$ J, respectively. Further,

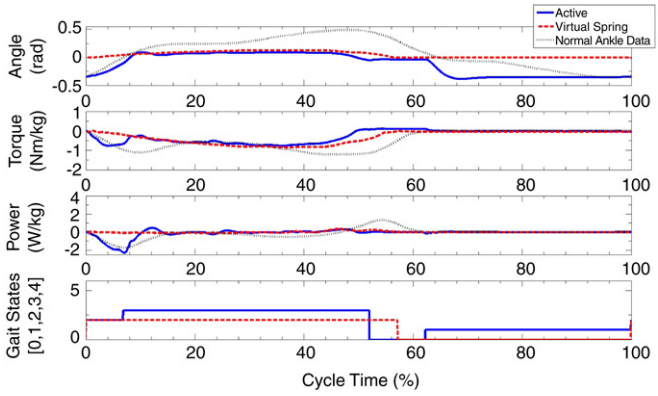

Fig. 11. Prosthetic ankle stair-descent performance. The solid blue, dotted red, and dotted grey lines represent the measured gait data for the active prosthetic condition (Active), the virtual spring condition (Virtual Spring), and the human ankle, respectively. The gait states for stair descent are defined as follows: CD1 = 2, CD2 = 3, SW0 = 0, and SW1 = 1. Data normalizations are equivalent to those used in Fig. 10. (For interpretation of the references to colour in this figure legend, the reader is referred to the web version of this article.)

the Active and Virtual Spring conditions resulted in peak powers during stance equal to 2.43 ± 0.06 W/kg and 1.47 ± 0.09 W/kg, respectively. All reported values are mean ± one STD for $N = 7$ walking trials.

3.2. Stair descent

Fig. 11 shows data for one complete gait cycle of stair descent for both the Active and Virtual Spring control conditions. The control states for stair descent are defined as follows: CD1 = 2, CD2 = 3, SW0 = 0 and SW1 = 1. Under the Virtual Spring condition, the state sequence was 0-2-0 (SW0-CD1-SW0), and while under the Active condition, the state sequence was 0-1-2-3-0 (SW0-SW1-CD1-CD2-SW0). Under the Active condition the prosthesis was controlled to planter flex to the desired equilibrium foot position of −0.35 rad (−20°) during terminal swing (SW1), so that during the early stance period (CD1) the prosthesis would provide negative power absorption and a greater shock attenuation compared to the Virtual Spring condition. The average net work done by the prosthesis for both the Active and Virtual Spring conditions were −14 ± 2 J and −0.10 ± 0.02 J, respectively.

3.3. Myoelectric-driven state transition

Fig. 12 shows an example of myoelectric recordings obtained during the participant training session, and model predictions of a sequence of dorsiflexion and plantar flexion commands. After the neural network had been trained, the proposed Neural Network Motor-Intent Estimator demonstrated the capacity to predict the desired ankle states. Fig. 13 shows that by using the estimator, the participant could voluntarily transition from level-ground to stair-descent gait patterns. When the participant flexed the gastrocnemius muscle at terminal swing, the prosthetic ankle plantar flexed to −0.35 rad (−20°) and the stair-descent state machine algorithm was initiated. To transition back to level-ground walking, the participant flexed his tibialis anterior muscle, keeping the ankle dorsiflexed at terminal swing, and initiating the level-ground state machine algorithm.

4. Discussion

4.1. Powered vs conventional passive-elastic prostheses

The human ankle is known to vary impedance within each level-ground walking cycle, across walking speed, and during stair descent and ascent (Gates, 2004; Hansen et al., 2004; Palmer, 2002; Winter, 1983). Furthermore, studies have indicated that one of the main functions of the human ankle is to provide net positive work during the stance period, especially at moderate to fast walking speeds (Gates, 2004; Hansen et al., 2004; Hof et al., 1983; Palmer, 2002; Winter, 1983). In distinction, conventional prostheses are passive while in contact with the ground surface, and are therefore incapable of biomimetic ankle dynamics. In this investigation we advance a powered ankle-foot prosthesis that captures biomimetic gait patterns for level-ground walking and stairs.

The preliminary study results suggest that a powered prosthesis (Active condition) can provide a more biomimetic ankle response in level-ground walking as compared to a passive spring prosthesis (Virtual Spring condition). The Active control condition resulted in a stance time, toe-off angle, and peak torque that agreed well with human values (see Fig. 10). Although the peak power output of the Active control condition was less than normal (prosthesis ∼2.4 W/kg; human ∼3 W/kg), the prosthesis nonetheless increased power output by 65% compared to the Virtual Spring control. In a separate study (Au, 2007; Au et al., in review, 2007b; Herr et al., 2007), the same powered prosthetic design (Active control condition) was shown to improve amputee metabolic economy on average by 14% compared to the conventional passive-elastic prostheses evaluated (Flex-Foot Ceterus and Freedom Innovations Sierra), even though the powered system was twofold heavier than the conventional devices.[3] This result highlights the benefit of a prosthesis that produces net propulsive work during level-ground walking.

For stair-descent ambulation, a normal human ankle behaves as a damper to absorb a significant amount of potential energy during the early stance period (Gates, 2004; McFadyen & Winter, 1988; Riener et al., 2002). Since conventional prostheses only provide a spring-like response during stance, active damping modulation cannot be achieved. Using the Active control condition, the prosthesis was found to absorb a considerable amount of mechanical energy in the early stance period of stair descent (−14 J), producing a more biomimetic ankle response (see Fig. 11). Using this control approach, the amputee participant reported a decrease in hip and knee effort during stair descent compared to the Virtual Spring control where very little mechanical energy was absorbed (−0.1 J). Additional kinematic and kinetic data from more amputee participants will be necessary to provide a more comprehensive and quantitative understanding of the effects of variable-damping on amputee stair-descent ambulation.

4.2. Prosthetic control system architecture

In addition to biomimetic ankle behavior, in this investigation we further seek an ankle-foot prosthesis that allows the amputee user to voluntarily select either level-ground or stair-descent prosthetic gait patterns through residual limb muscle activation. The use of a finite state machine that employs only local prosthetic sensory information seems effective for producing biomimetic ankle behaviors within a particular gait pattern that is highly periodic in nature. Clearly, the local nature of the level-ground and stair-descent controllers has practical advantages. Since the controllers require only sensory information from the external prosthesis, one avoids having to place sensors on other parts of the body such as, for example, the unaffected leg of a unilateral patient.

[3] In this study, metabolic economy was measured for three unilateral transtibial amputees walking on level ground at self-selected speeds using the powered prosthesis and conventional prostheses. Here economy refers to the metabolic energy required to transport unit body weight, unit distance. Metabolic energy was estimated from measures of oxygen consumption and carbon dioxide production.

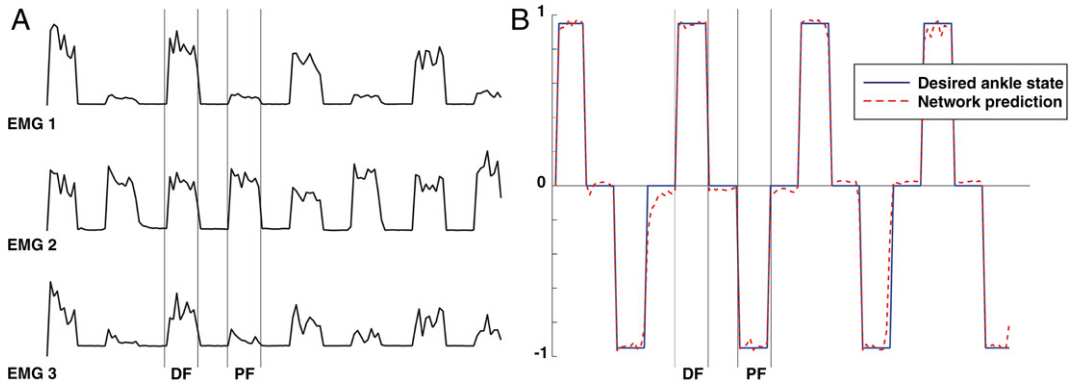

Fig. 12. In (A), sample myoelectric recordings obtained during the participant's training procedure. The variances of myoelectric signals labeled EMG1, EMG2 and EMG3 were obtained by placing electrodes over the approximate locations of the participant's tibialis anterior and gastrocnemius muscles, respectively. The electrodes used to measure the EMG2 and EMG3 signals were positioned at two distinct locations on the gastrocnemius muscle, one medial and one lateral. Typical periods of activity during a phantom limb command of dorsiflexion (DF) and plantar flexion (PF) are indicated in (A). In (B), shown are predictions of motor intent obtained after neural network training (dashed line). Dorsiflexion is indicated with a value of one, plantar flexion with a value of negative one, and the relaxed state with a value of zero. Also shown are the desired ankle states used to train the network (solid line).

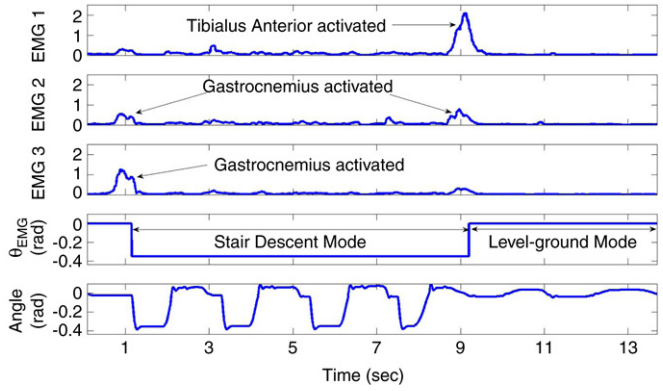

Fig. 13. The participant could voluntarily select one prosthetic state controller over another by flexing residual limb muscles. When the gastrocnemius was activated at 1 s, the prosthetic ankle plantar flexed to −0.35 rad (−20°) at terminal swing, initiating the stair-descent state machine algorithm with $\theta_{\text{EMG}} = -0.35$ rad. To transition back to level-ground walking, the participant flexed the tibialis anterior at 9 s, keeping the ankle dorsiflexed at terminal swing, and initiating the level-ground state machine algorithm with a $\theta_{\text{EMG}} = 0$ rad.

However, to maintain natural and smooth transitions from one terrain to another is difficult with only local prosthetic sensing. Today's active leg prostheses detect terrain variations too slowly, normally requiring at least one step delay before a control action is taken (Ossur, 2002–2008). Our approach of using the residual limb myoelectric signals as control commands allows a quicker control mode transition. Furthermore, since the myoelectric signals are only interpreted with a binary level control, the estimator design is simplified and is less susceptible to noise. In this investigation, the surface electrodes were positioned within the residual limb socket — between the amputee's skin and a silicone liner. Thus, due to this type of electrode placement a far greater movement artifact was expected in the myoelectric signal. Even under these conditions, we found that the amputee could robustly transition between local state controllers through direct muscle activation (see Fig. 13). These results highlight the potential of prosthetic leg controllers that exploit myoelectric signals to trigger terrain-appropriate, local prosthetic leg behaviors.

4.3. Powered plantar flexion control

It is still unclear what kind of powered plantar flexion strategy would be most effective for amputee locomotion. The method of using a constant offset torque was an initial attempt to mimic the active plantar flexion of normal human walking. It was not our intent to capture all the nonlinear characteristics of the observed quasi-static stiffness curve or power characteristics of the normal human ankle in walking. A consequence of such a control strategy was that the measured power output profile of the prosthesis during powered plantar flexion was somewhat different from that of a normal human ankle. As shown in Fig. 10, two power splits or hubs are present at terminal stance for the prosthesis that do not appear in human walking. Nevertheless, the control strategy presented in this investigation reduced the number of control parameters and provided for a more intuitive way to relate the amputee's feedback to control parameter adjustments.

4.4. Gait symmetry

In this investigation, asymmetry was observed in the gait of the bilateral amputee participant. In particular, a larger knee flexion during late stance was observed on the trailing right leg as compared to that on his leading left leg. We believe this asymmetry occurred mainly because the active push-off generated by the powered prosthesis on his right leg caused the right knee joint to flex to a larger extent during late stance. It is noted that the participant wore the powered prosthesis on his right leg and a conventional passive prosthesis (Flex-Foot Ceterus® from Ossur, Inc.) on his left leg. We suspect that this asymmetry may not have occurred had the bilateral amputee used a powered prosthesis on both legs.

5. Future work

In future work we plan to conduct a comprehensive biomechanical gait study involving more amputee participants, including the measurement of metabolic, electromyographic, kinematic and kinetic gait data. Such a biomechanical investigation will provide a quantitative understanding of the affects of prosthetic ankle power on amputee locomotion. We also wish to develop additional finite state controllers for other locomotory modes, such as stair ascent or ramp climbing. Additionally, we hope to further exploit myoelectric signals as control commands to manage the switching between finite state controllers appropriate for a large repertoire of locomotory terrains and conditions. It is our hope that this work will motivate additional studies focused on the advancement of multifunctional lower-extremity prostheses.

Acknowledgements

This research was supported by the US Veterans Administration under Grant VA241-P-0026. The authors would like to acknowledge the contributions of MIT researchers Chris Barnhart, Bruce Deffenbaugh, and Jeff Weber for their invaluable electromechanical design work.

References

Abul-haj, C. J., & Hogan, N. (1990). Functional assessment of control systems for cybernetic elbow prostheses. Part I, Part II. *IEEE Transactions on Biomedical Engineering*, *37*(11), 1025–1047.

Akazawa, K., Okuno, R., & Yoshida, M. (1996). Biomimetic EMG prosthesis-hand. In *Proceedings of the 18th annual international conference of the IEEE engineering in medicine and biology society, Vol. 2* (pp. 535–536).

Au, S. K. (2007). Powered ankle-foot prosthesis for the improvement of amputee walking economy. *Ph.D. thesis*. Massachusetts Institute of Technology.

Au, S. K., Bonato, P., & Herr, H. (2005). An EMG-position controlled system for an active ankle-foot prosthesis: an initial experimental study. In *Proc. IEEE international conference on rehabilitation robotics* (pp. 375–379).

Au, S. K., Dilworth, P., & Herr, H. (2006). An ankle-foot emulation system for the study of human walking biomechanics. In *Proc. IEEE int. conf. on robotics and automation* (pp. 2939–2945).

Au, S. K., & Herr, H. (2006). Initial experimental study on dynamic interaction between an amputee and a powered ankle-foot prosthesis. In *Workshop on dynamic walking: Mechanics and control of human and robot locomotion*.

Au, S. K., Weber, J., & Herr, H. (2007a). Biomechanical design of a powered ankle-foot prosthesis. In *Proc. IEEE int. conf. on rehabilitation robotics* (pp. 298–303).

Au, S. K., Weber, J., & Herr, H. (2008). Powered ankle-foot prosthesis improves walking metabolic economy. *IEEE Robotics and Automation* (in review).

Au, S. K., Weber, J., Martinez-Villapando, E., & Herr, H. (2007b). Powered ankle-foot prosthesis for the improvement of amputee ambulation. In *IEEE engineering in medicine and biology international conference* (pp. 3020–3026).

Bateni, H., & Olney, S. (2002). Kinematic and kinetic variations of below-knee amputee gait. *Journal of Prosthetics & Orthotics*, *14*(1), 2–13.

Colborne, G. R., Naumann, S., Longmuir, P. E., & Berbrayer, D. (1992). Analysis of mechanical and metabolic factors in the gait of congenital below knee amputees. *American Journal of Physical Medicine and Rehabilitation*, *92*, 272–278.

Collins, S. H., & Kuo, A. D. (2003). Controlled energy storage and return prosthesis reduces metabolic cost of walking. In *Proc. on ISB XXth congress and the American society of biomechanics annual meeting* (p. 804).

Doerschuk, P. C., Gustafson, D. E., & Willsky, A. (1983). Upper extremity limb function discrimination using EMG signal analysis. *IEEE Transactions on Biomedical Engineering*, *30*(1), 18–28.

Farry, K. A., et al. (1996). Myoelectric teleoperation of a complex robotic hand. *IEEE Transactions on Robotics and Automation*, *12*(5), 775–788.

Fukuda, O., et al. (2003). A human-assisting manipulator teleoperated by EMG signals and arm motions. *IEEE Transactions on Robotics and Automation*, *19*(2), 210–222.

Gates, D. (2004). Characterizing ankle function during stair ascent, descent, and level walking for ankle prosthesis and orthosis design. *Masters thesis*. Boston University, Boston.

Graupe, D., et al. (1978). A microprocessor system for multifunctional control of upper-limb prostheses via myoelectric signal identification. *IEEE Transaction on Automatic Control*, *AC-23*(4), 538–544.

Grimes, D. L. (1976). An active multi-mode above-knee prosthesis controller. *Ph.D. thesis*. Massachusetts Institute of Technology.

Hansen, A. H. et al. (2007). Automatically-adapting ankle-foot prosthesis concept. In *12th world congress of the international society for prosthetics and orthotics*.

Hansen, A., Childress, D., Miff, S., Gard, S., & Mesplay, K. (2004). The human ankle during walking: Implication for the design of biomimetic ankle prosthesis. *Journal of Biomechanics*, *37*(10), 1467–1474.

Herr, H., Paluska, D., Dilworth, P., & Au, S. (2005). Inventors; A hybrid actuator comprising motor, spring and variable-damper elements. *Patent provisional F-51 SN 60/666,876*.

Herr, H., Weber, J., & Au, S. K. (2007). Powered ankle-foot prosthesis. In *Biomechanics of the lower limb in health, disease and rehabilitation*. Manchester, England (pp. 72–74).

Herr, H., & Wilkenfeld, A. (2003). User-Adaptive Control of a Magnetorheological Prosthetic Knee. *Industrial Robot: An International Journal*, *30*, 42–55.

Hirai, K. et al. (1998). The development of Honda humanoid robot. In *Proc. on IEEE/RSJ int. conf. on intelligent robots and systems* (pp. 1321–1326).

Hitt, J., Bellman, R., Holgate, M., Sugar, T., & Hollander, K. (2007). The Sparky (Spring Ankle with regenerative Kinetics) projects: Design and analysis of a robotic transtibial prosthesis with regenerative kinetics. In *ASME international design engineering technical conference, CD-ROM* (pp. 1–10).

Hof, A. L., Geelen, B. A., & Van den Berg, Jw. (1983). Calf muscle moment, work and efficiency in level walking; role of series elasticity. *Journal of Biomechanics*, *16*(7), 523–537.

Hogan, N. (1976). A review of the methods of processing EMG for use as a proportional control signal. *Biomedical Engineering*, 81–86.

Huang, H. P., & Chen, C. Y. (1999). Development of a myoelectric discrimination system for a multi-degree prosthetic hand. In *Proceeding of the IEEE international conference on robotics and automation* (pp. 2392–2397).

Inman, V. T., Ralston, H. J., & Todd, F. (1981). *Human walking*. Baltimore: Williams and Wilkins.

Kaneko, K. et al. (2004). Humanoid robot HRP-2. In *Proc. IEEE int. conf. on robotics and automation* (pp. 1083–1090).

Klute, G. K., Czerniecki, J., & Hannaford, B. (1998). Development of powered prosthetic lower limb. In *Proc. 1st national mtg, veterans affairs rehab. R&D service*.

Koganezawa, K., & Kato, I. (1987). Control aspects of artificial leg. *IFAC Control Aspects of Biomedical Engineering*, 71–85.

Li, C. et al. (2006). Research and development of the intelligently-controlled prosthetic ankle joint. In *Proc. of IEEE int. conf. on mechatronics and automation* (pp. 1114–1119).

McFadyen, B. J., & Winter, D. A. (1988). An integrated biomechanical analysis of normal stair ascent and descent. *Journal of Biomechanics*, *21*(9), 733–744.

Molen, N. H. (1973). Energy/speed relation of below-knee amputees walking on motor-driven treadmill. *European Journal of Applied Physiology*, *31*(3), 173–185.

Palmer, M. (2002). Sagittal plane characterization of normal human ankle function across a range of walking gait speeds. *Masters thesis*. Massachusetts Institute of Technology, Cambridge.

Pratt, G. A., & Williamson, M. M. (1995). Series elastic actuators. In *Proceedings on IEEE/RSJ international conference on intelligent robots and systems. pittsburgh, Vol. 1* (pp. 399–406).

Riener, R., Rabuffetti, M., & Frigo, Carlo. (2002). Stair ascent and descent at different inclinations. *Gait Posture*, *15*, 32–44.

Robinson, D. (2000). Design and an analysis of series elasticity in closed-loop actuator force control. *Ph.D. thesis*. Massachusetts Institute of Technology.

Ron, S. (2002). *Prosthetics and orthotics: Lower limb and spinal*. Lippincott Williams & Wilkins.

Rosen, J., et al. (2001). A myosignal-based powered exoskeleton system. *IEEE Transactions on Systems, Man, and Cybernetics-Part A: Systems and Humans.*, *31*(3), 210–222.

Skinner, H. B., et al. (1985). Gait analysis in amputees. *American Journal of Physical Medicine*, *64*, 82–89.

© Ossur 2002–2008. www.ossur.com.

US Patent 6443993. Sept. 3, 2002.

Versluys, R. et al. (2007). Design of a powered below-knee prosthesis. In *12th world congress of the international society for prosthetics and orthotics*.

Winter, D. A. (1983). Biomechanical motor pattern in normal walking. *Journal of Motor Behavior.*, *15*(4), 302–330.

Winter, D. A., & Sienko, S. E. (1988). Biomechanics of below-knee amputee gait. *Journal of Biomechanics*, *21*(5), 361–367.

Zlatnik, D., Steiner, B., & Schweitzer, G. (2002). Finite-state control of a transfemoral prosthesis. *IEEE Transactions on Control System Technology*, *10*(3), 408–420.